Cyanide-Bridged Arrays of 2, 3 and 4 Metal Atoms Based on Salene–Iron Complexes – Syntheses, Structures and Metal–Metal Interactions

Andreas Geiß[a] and Heinrich Vahrenkamp*[a]

Dedicated to Professor Wolf-Peter Fehlhammer on the occasion of his 60th birthday

Keywords: Iron complexes / Salene ligands / Cyanide bridging / Electron transfer / Metal–metal interactions

Salene–Fe^{III} complexes of the types LFeCl and $[LFe(CN)_2]^-$ were treated with organometallic reagents to introduce the cyanide-linked units $(CO)_5Cr$, $(CO)_5Mo$, $(CO)_5W$, $Cp(CO)_2Fe$, Cp(dppe)Fe, and $Cp(PPh_3)_2Ru$. IR spectra and structure determinations revealed that all resulting complexes contained M–CN units with N coordination to the salene–Fe units. They were either dinuclear M–CN–Fe(salene), trinuclear M–CN–Fe(salene)–NC–M, or tetranuclear M–CN–Fe(salene)–Fe(salene)–NC–M species. Cyclic voltammetry showed that there are significant electronic interactions between the two outer organometallic units in the trinuclear complexes. UV/Vis spectra indicated a metal–metal charge transfer from the outer Cp(dppe)Fe groups to the central Fe^{III}. The magnetic moments at room temperature of the tri- and tetranuclear complexes are slightly lower than those calculated for isolated high-spin Fe^{III} species.

In the previous papers of this series[1][2] and in a feature article[3] we have outlined our interest in complexes containing cyanide-bridged arrays of redox-active transition metal ions. Our aim is to elucidate the factors determining the extent of electronic interactions between remote metal centers in such arrays. Our preparative approach consists of constructing the arrays from cyanometal complexes L_nM-CN and complexes $L_nM'-X$ containing labile ligands X. This approach allows a wide variation of L, M and X, as well as of the geometrical relation between two cyanide bridges at a central metal ion (*cis*, *trans*, tetrahedral, etc.), and of the orientations of the cyanide bridges (cyanide vs. isocyanide). The techniques used to assess the metal–metal interactions include IR spectroscopy, cyclic voltammetry, preparative redox chemistry, magnetic measurements and NIR spectroscopy. Our main contribution to this area is the design and variation of suitable new compounds, the investigation of which extends the work of previous researchers in the field.[3]

So far we have gained basic knowledge by studying dinuclear M–CN–M′ complexes and then applied this knowledge to include symmetrical trinuclear complexes of the types $M(CN-M')_2$ or $M(NC-M')_2$.[2,4,5] One important finding from these studies is that, as expected, a linear array of M–CN units allows for much better remote interactions than bent arrays. This was verified by finding an interaction between the terminal metal ions in a tetranuclear complex that was obtained accidentally.[6] Accordingly, we focused our preparative efforts on building blocks that only allow a *trans* arrangement of cyanide bridges at a connecting metal center. In essence this means the use of disc-like L_nM units with planar tetradentate ligands L_n as building blocks, as already applied some years ago by Hanack for the synthesis of electrically conducting [(Pc)M–CN] polymers (Pc = phthalocyanine).[7]

For the present investigation we chose salene ligands to ensure square-planar metal coordination of the central metal ions. The advantage of these ligands is their easy accessibility and variability, as well as the fact that they are good coligands for both square-pyramidal L^4M-X and octahedral $X-ML^4-Y$ complexes.[8] Our aim was to construct linear multinuclear arrays by using cyanide for X and Y. This paper describes our results obtained with salene–iron units. Iron was chosen as the central metal because of its redox properties. The tetradentate ligands were either salene itself (**L1**) or its bis(methoxy)-substituted variant vanene (**L2**) (Scheme 1).

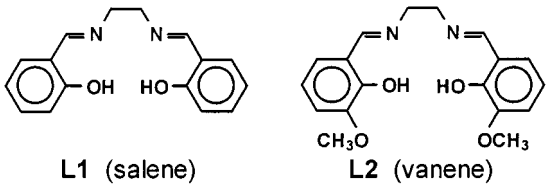

L1 (salene) **L2** (vanene)

Scheme 1

Preparations

The starting iron complexes with salene ligands were **1a**,**b**, and **2a**,**b**.[9] We expected the former to lead to CN-bridged arrays with (salene)Fe–N coordination and the latter to maintain their (salene)Fe–C coordination upon attachment of other metals to the cyanide ligands.

(**L1**)Fe–Cl **1a**	K[(**L1**)Fe(CN)$_2$] **2a**
(**L2**)Fe–Cl **1b**	K[(**L2**)Fe(CN)$_2$] **2b**

[a] Institut für Anorganische und Analytische Chemie der Universität Freiburg,
Albertstraße 21, D-79104 Freiburg, Germany
Fax: (internat.) + 49-(0)761/203-6001
E-mail: vahrenka@uni-freiburg.de

  1434–1948/99/1010–1793 $ 17.50+.50/0

Complexes **1** were treated with the monofunctional cyanometal complexes **3**−**8** with the aim of replacing the halide by the cyanometal "ligands" and possibly attaching a second cyanometal unit to form trinuclear species.

$Cp(CO)_2Fe-CN$ **3**

$Na[(CO)_5Cr-CN]$ **6**

$Cp(dppe)Fe-CN$ **4**

$Na[(CO)_5Mo-CN]$ **7**

$Cp(PPh_3)_2Ru-CN$ **5**

$Na[(CO)_5W-CN]$ **8**

Conversely, complexes **2** were reacted with the monofunctional species **9**−**11**, which are the sources of the cationic electrophiles $Cp(L_2)M$ to be attached at the N terminus of the cyanide ligands.

$[Cp(CO)_2Fe(THF)]PF_6$ **9**

$[Cp(dppe)Fe(CH_3CN)]Br$ **10**

$Cp(PPh_3)_2Ru-Cl$ **11**

All 1:1 combinations between complexes **1** and reagents **4**−**8** in methanol led to products with an Fe/M ratio of 1:1. In only one case, however, was such a product isolated as a simple dinuclear complex: The two most volumious partners, **1b** and **5**, yielded **12**, whose constitution was confirmed by a structure determination of its PF_6^- salt.

$[(H_2O)(\mathbf{L2})Fe-NC-Ru(PPh_3)_2Cp]^+$ **12**

In all other cases the 1:1 products were found to be associated with dimeric entities, i.e. tetranuclear complexes, in the solid state. This was ascertained by structure determinations of **[13a]**$(PF_6)_2$ and **[13a]**$(BPh_4)_2$ and deduced from the spectral similarities and solubility properties for the other complexes. This behavior corresponds to that of **1a**, which is also dimeric in the solid state but probably monomeric in polar solvents.[9][10] Complexes **13**−**17** were isolated and, of these, the ionic ones (**13**, **14**) could be crystallized as ClO_4^-, PF_6^-, SbF_6^- or BPh_4^- salts upon addition of the corresponding counterions.

$[(\mathbf{L})Fe-NC-Fe(dppe)Cp]_2^{2+}$ **13a**: L = **L1**; **13b**: L = **L2**

$[(\mathbf{L1})Fe-NC-Ru(PPh_3)_2Cp]_2^{2+}$ **14**

$[(\mathbf{L1})Fe-NC-M(CO)_5]_2$ **15**: M = Cr; **16**: M = Mo; **17**: M = W

Some of the tetranuclear dimers **13**−**17** were also precipitated from solutions containing two equivalents of the cyanometal reagents per equivalent of starting complex **1**. By adjusting the reaction conditions, however, the expected trinuclear complexes with two cyanometal "ligands" could be isolated. Starting from **1a** and **1b** these were **18a**, **18b**, **20a**, **21**, **22**, and **23**. Of these, the cationic compounds (**18**, **20**) could again be precipitated with one or several of the four anions named above, while the anionic ones (**21**−**23**) were precipitated as PPh_4^+ salts. Their trinuclear nature was ascertained by a structure determination of **[20a]**PF_6.

$(\mathbf{L})Fe\{NC-Fe(CO)_2Cp\}_2]^+$ **18a**: L = **L1**; **18b**: L = **L2**

$[(\mathbf{L})Fe\{NC-Fe(dppe)_2Cp\}_2]^+$ **19a**: L = **L1**; **19b**: L = **L2**

$[(\mathbf{L})Fe\{NC-Ru(PPh_3)_2Cp\}_2]^+$ **20a**: L = **L1**; **20b**: L = **L2**

$[(\mathbf{L})Fe\{NC-M(CO)_5\}_2]^-$ **21**: M = Cr; **22**: M = Mo; **23**: M = W

Attempts to obtain complexes like **13**−**21** with an inverted orientation of the bridging cyanide ligands by using **2a** and **2b** as starting materials were unsuccessful. Invariably the Fe^{III}-attached cyanide ligands of **2a** and **2b** were turned around upon attachment of the other organometallic units. Thus **18a**, **19a**, and **20a** were obtained as PF_6^- salts from **2a**, and **9**, **10**, or **11**. Likewise, **19b** and **20b** resulted, though not in a pure form, from **2b** and **10** or **11**.

The formation of the isolated complexes can be understood from the solution behavior of the simple salene−Fe^{III} complexes.[8−11] It is known that **1a** and **1b**, which are molecular dimers in the solid state, are solvated and probably ionized in solution, being engaged in a monomer-dimer equilibrium as shown in Equation 1. This equilibrium should depend on the solvent, on other donor ligands, on the anions present, and on the solubility of the various species. The monomer **A**, with X = CH_3OH, would represent the simplest species in methanol solutions of **1a** or **1b**. For X = CN^- complex **A** would be the intact starting material **2a** or **2b**. Partial replacement of the labile ligands X from **A** or **B** could change the total charge of the solution species and hence their solubility or their preference in the equilibrium.

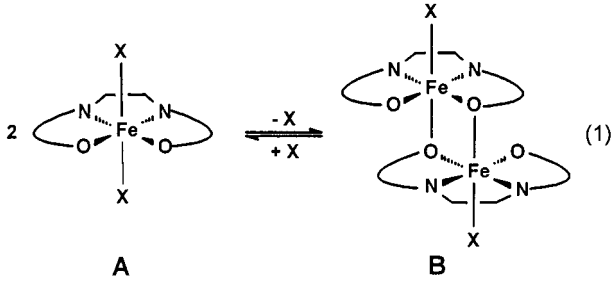

(1)

Of the isolated complexes, the 1:1 species **13**−**17** show their dimeric nature by their lower solubility compared to the 1:2 species **18**−**23**, which for **13** and **14** also corresponds to a dipositive charge of the complex cations. Steric effects are evident from the fact that the most voluminous cyanometal "ligand" **5** does not want to form a 1:2 complex (**20b**) starting from (**L2**)FeCl, but rather the unique 1:1 complex **12**. Likewise, the least voluminous cyanometal "ligand" **3** could not be incorporated into a 1:1 complex, but easily formed the 1:2 complexes **18a** and **18b**. Electronic effects can also be invoked to explain the lower tendency for the formation of **20b** in comparison to **20a**: The vanene ligand (**L2**) is more electron-rich than the salene ligand (**L1**), and hence the Fe^{III} ion coordinated by it is less prone to bind a sixth donor. The low binding tendency of all (**L1**)Fe−X or (**L2**)Fe−X complexes for a sixth donor ligand also provides

an explanation for the inversion of the cyanide attachment to the Fe^{III} center in **2a** and **2b** upon complexation to the incoming organometallic units. This feature allows the liberation of CN^- in solution, which also makes the crystallization of dimeric (salene)Fe−CN possible.[12]

Structures

One representative example of each structural type was subjected to X-ray analysis. In the case of **13a** the complex salts with either PF_6^- or BPh_4^- as counterions differed so much in their ν(CN) IR data (see below) that it seemed worthwhile to explain this phenomenon in terms of their structures.

Compound [**12**]SbF_6 (see Figure 1) is the only species in this report that is dinuclear in the solid state and that bears a ligand other than cyanide or salene on the central Fe^{III} ion. The coordination geometries in **12** [distorted octahedral at Fe^{III}, piano stool at Ru] are normal. The salene ligand **L2** defines a square-planar environment of the iron center to a good approximation and can itself be described by the "stepped" conformation.[8][11] The Fe−O(water) distance of 2.18 Å is significantly longer than the Fe−O(salene) distances (av. 1.89 Å), while the Fe−N(cyanide) distance (2.05 Å) is a little shorter than the Fe−N(salene) distances (av. 2.08 Å).

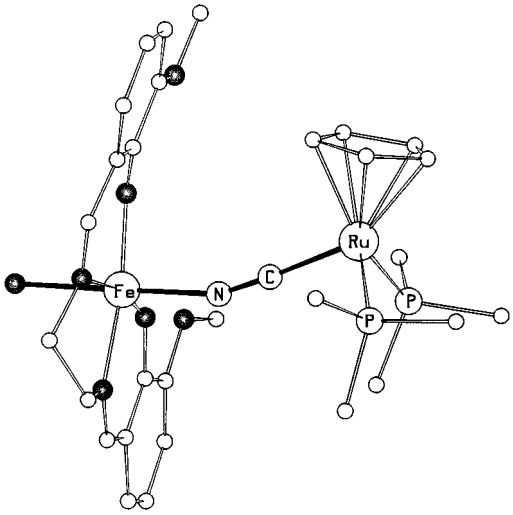

Figure 1. Structure of complex **12** in [**12**]SbF_6; Selected bond lengths [Å] and angles [°]: Fe−O(salene) 1.885(7) and 1.902(7), Fe−N(salene) 2.083(9) and 2.076(9), Fe−O(H_2O) 2.184(6), Fe−N(CN) 2.046(8), C−N(CN) 1.13(1), Ru−C(CN) 1.973(10); Fe−N−C(CN) 160.1(9), R−C−N(CN) 176.4(9)

The bridging cyanide ligand in **12** shows typical features. Its π-acceptor terminus, the C atom, is naturally bound to the electron-rich ruthenium atom as it is the better π donor. This is reflected by the Ru−C distance, which is shorter than the Fe−N distance on the other side. Likewise, the Ru−C−N angle (176°) is much closer to linearity than the Fe−N−C angle (160°). These two indicators of the π-bonding abilities of the C and N atoms of the cyanide ligand, as well as of the metal centers attached to them, have been found to be of good diagnostic value.[1−3]

The two complex salts derived from **13a**, containing PF_6^- and BPh_4^- as counterions, were both found to have the dimeric units of **13a** in the solid state. The structure determination of [**13a**]$(PF_6)_2$ resulted in an unsatisfactory *R* value of 0.119, and only the structure of [**13a**]$(BPh_4)_2$ is discussed in detail here (see Figure 2). The dimer **13a** is centrosymmetrical in both compounds. As usual for such salene complex dimers,[8][11] one each of the salene oxygen atoms is used to bridge the two monomer units resulting in a central Fe_2O_2 square, and the salene ligands once again have the "stepped" conformation.

The bonding characteristics of the bridging cyanide ligands compare closely with those in **12**, both in terms of metal−cyanide bond lengths and of the angles at C and N. There is ample precedence for bridging cyanide coordinated to the iron center at the C and N terminus,[1][2] including Prussian Blue.[13] The Fe′−C distance in **13a** compares well with other Fe−C distances in Cp(dppe)Fe−CN derivatives, but the Fe−N distance in **13a** is larger than other such distances in complexes of low-valent iron. It is, however, comparable to the Fe^{III}−N distance in Prussian Blue.

The two major differences between the shapes of the dimeric units **13a** in [**13a**]$(BPh_4)_2$ and [**13a**]$(PF_6)_2$ lie in the bending of the Fe−CN−Fe bridge and the relative orientation of the Fe(salene) units with respect to the Fe(dppe)Cp units. The latter in [**13a**]$(PF_6)_2$ are rotated by about 30° around the Fe−CN−Fe′ line compared to [**13a**]$(BPh_4)_2$. More significant is the difference in the Fe−N−C angles, which are 152° in [**13a**]$(BPh_4)_2$ and 178° in [**13a**]$(PF_6)_2$. The voluminous tetraphenylborate counterions seem to cause severe bending of the "soft" Fe−N−C angles, which in turn is the reason for the lowering of ν(CN) in [**13a**]$(BPh_4)_2$ (see below).

Compound [**20a**]PF_6 has an approximately linear Ru−CN−Fe−NC−Ru arrangement in the solid state (see Figure 3). Its general features can be compared with those of [**12**]SbF_6: The central Fe^{III} ion has a roughly octahedral coordination, its "stepped" salene ligand comprises a roughly square-planar FeO_2N_2 arrangement, and the attachment of the $Cp(PPh_3)_2Ru$−CN "ligands" is similar. The second $Cp(PPh_3)_2Ru$−CN unit in [**20a**]PF_6 occupies the position of the water ligand in [**12**]SbF_6 but is not symmetry-related to the first one.

The attachment of two cyanometal units to the (salene)-Fe^{III} center leads to different bonding characteristics of the bridging cyanide ligands in **20**. Compared to **12** the central Fe−N bonds are 0.05 Å longer, which may point to a *trans* effect, while the Ru−C(cyanide) bond lengths in both complexes are virtually identical. The bending of the Fe−N−C(cyanide) angles in **20** is less pronounced than in **12**, while the bending of the Ru−C−N(cyanide) angles is more pronounced. However, since all four angles Fe−N−C and Ru−C−N are bent in the same direction, the total deviation of the Fe−N−C−Ru sequences from linearity (18−24°) is the same in both complexes. Indeed, in **20** all

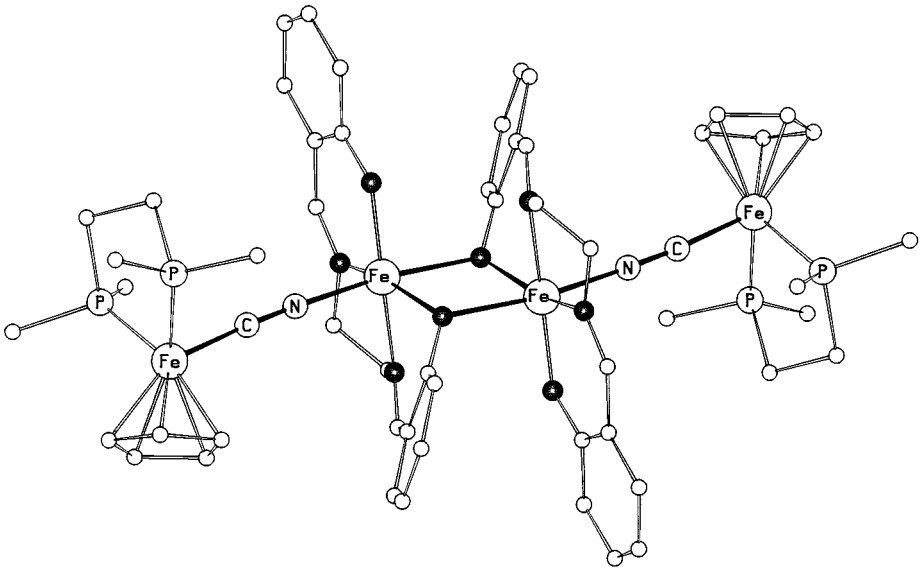

Figure 2. Structure of complex **13a** in [**13a**]$(BPh_4)_2$; selected bond lengths [Å] and angles [°]: Fe−O(unbridged) 1.876(4), Fe−O(bridge) 1.991(4), Fe−O′(bridge) 2.117(4), Fe−N(salene) 2.091(5) and 2.123(5), Fe−N(CN) 2.017(5), C−N(CN) 1.161(7), Fe′−C(CN) 1.817(7), Fe− − −Fe(across bridge) 4.835(2); O−Fe−O(bridge) 78.4(2), Fe−O−Fe(bridge) 101.6(2), Fe−N−C(cyanide) 151.5(5), Fe′−C−N(cyanide) 178.2(6)

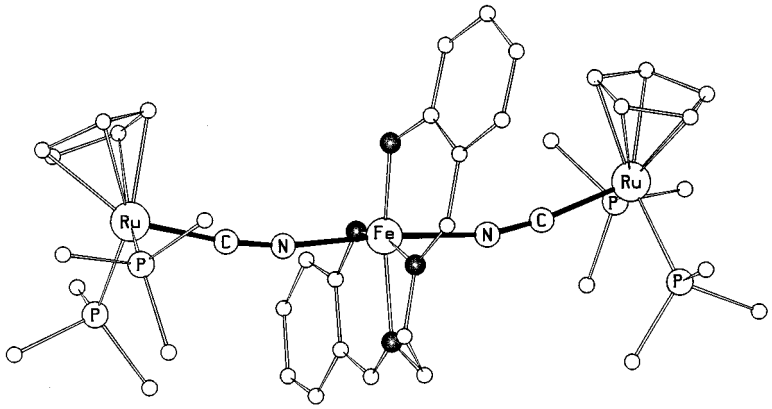

Figure 3. Structure of complex **20** in [**20**]PF_6; selected bond lengths [Å] and angles [°]: Fe−O(salene) 1.902(3) and 1.925(4), Fe−N(salene) 2.128(4) and 2.102(4), Fe−N(CN) 2.092(4) and 2.092(4), C−N(CN) 1.151(5) and 1.162(6), Ru−C(CN) 1.965(4) and 1.961(4); N−Fe−N-(cyanide) 174.3(2), Fe−N−C(cyanide) 166.1(4) and 169.9(4), Ru−C−N(cyanide) 170.5(4) and 172.3(4)

atoms of the Ru−CN−Fe−NC−Ru sequence lie approximately in one plane.

IR Data

The ν(CO) data of the complexes with carbonyl ligands are listed in the Experimental Section. The ν(CN) values are given in Table 1 for the solid state and for solutions.

Based on the accumulated experience with oligonuclear complexes of the cyanometal "ligands" **3**−**8**[1,2,4,5] and on the cross-comparison of the data in Table 1, several unambiguous conclusions can be drawn about the structure and bonding in the complexes described here. The simplest of these can be derived from the observation that, with few exceptions (**18a**,**b**), the ν(CN) values are lower in the bridged complexes than in the free metallocyanides **3**−**8**. This means that the kinematic effect [constraint of CN motion by double attachment, i.e. raising of ν(CN)] is outweighed by an electronic effect. The latter consists in the electron withdrawal at the N terminus of the CN by the electron-poor Fe^{III} center, which in turn causes enhanced π-backdonation from the electron-rich organometallic units at the C terminus into the π* orbitals of the C−N bond, and hence a weakening of this bond. Proof for this is found in the ν(CO) values of the "ligands" **3**, **6**, **7**, and **8**, which are raised upon formation of the oligonuclear complexes.

The data for the dimeric 1:1 complexes **13a**, **13b** and **14** indicate that the amount of π-backdonation seems to depend on structural details. The solid-state IR spectra of these complexes show a marked dependence of ν(CN) upon the counterion present. This is most evident for **13a**, which experiences a decrease of 20 cm^{-1} in ν(CN) on going from the smallest (ClO_4^-) to the largest counterion (BPh_4^-). As seen from the structure determinations (see above) this

Table 1. IR data ν(CN) [cm^{-1}]

	L_nM'[a]	In KBr	In solution[b]
3	$Cp(CO)_2Fe$	2116	C: 2119
4	Cp(dppe)Fe	2062	C: 2062
5	$Cp(PPh_3)_2Ru$	2072	C: 2072
6	$(CO)_5Cr$	2108	M: 2103
7	$(CO)_5Mo$	2107	M: 2103
8	$(CO)_5W$	2111	M: 2104
[**12**]PF_6	$Cp(PPh_3)_2Ru$	2063	C: 2061
[**12**]SbF_6	$Cp(PPh_3)_2Ru$	2061	C: 2061
[**13a**]ClO_4	Cp(dppe)Fe	2058	C: 2013
[**13a**]PF_6	Cp(dppe)Fe	2048	C: 2013
[**13a**]SbF_6	Cp(dppe)Fe	2052	C: 2013
[**13a**]BPh_4	Cp(dppe)Fe	2039	C: 2013
[**13b**]PF_6	Cp(dppe)Fe	2058	C: 2014
[**13b**]SbF_6	Cp(dppe)Fe	2056	C: 2014
[**14**]PF_6	$Cp(PPh_3)_2Ru$	2055	C: 2029
[**14**]SbF_6	$Cp(PPh_3)_2Ru$	2054	C: 2029
[**14**]BPh_4	$Cp(PPh_3)_2Ru$	2051	C: 2029
15	$(CO)_5Cr$	2097	M: 2099
16	$(CO)_5Mo$	2102	M: 2104
17	$(CO)_5W$	2104	M: 2106
[**18a**]ClO_4	$Cp(CO)_2Fe$	2134	C: 2137
[**18b**]SbF_6	$Cp(CO)_2Fe$	2132	C: 2133
[**19a**]PF_6	Cp(dppe)Fe	2063	C: 2059
[**19b**]SbF_6	Cp(dppe)Fe	2057	C: 2054
[**20a**]PF_6	$Cp(PPh_3)_2Ru$	2076	C: 2072
[**20b**]SbF_6	$Cp(PPh_3)_2Ru$	2071	C: 2069
[**21**]PPh_4	$(CO)_5Cr$	2114	M: 2102
[**22**]PPh_4	$(CO)_5Mo$	2115	M: 2104
[**23**]PPh_4	$(CO)_5W$	2119	M: 2107

[a] Terminal organometallic unit. − [b] C: dichloromethane, M: methanol.

corresponds to an increased bending of the C−N−Fe^{III} linkage at the nitrogen atom. In accord with similar observations for Fe−CN−Cu systems[14] a simplistic explanation for this may be proposed by formulating an angle-dependent variation between a C−N double bond and a C−N triple bond according to the resonance formula in Scheme 2.

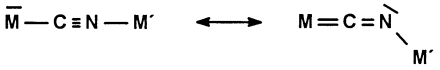

Scheme 2

Complexes **13** and **14** also show significantly different ν(CN) values in the solid state and in solution, and their solution IR data are not dependent on the counterions present. While their tetranuclear nature in the solid state was proved by the structure determinations, this indicates that in solution they are dinuclear, i.e. monomeric. This is in accord with the electrochemical data (see below). It is also supported by the fact that **12**, the only monomeric complex of this type, shows the same ν(CN) values in the solid state and in solution and for both counterions. Unlike **13** and **14**, the uncharged 1:1 complexes **15**−**17** show the same ν(CN) values in the solid state and in solution and, furthermore, in solution their ν(CN) values are virtually identical to those of the free metallocyanides **6**−**8**. In the absence of further indicators (no structures, no good electrochemical data) it cannot be concluded whether they are tetrameric in both the solid state and in solution or dissociate to yield the free metallocyanides in solution.

The ν(CN) data of the trinuclear complexes **19** and **20** are characteristically different from those of their (in solution) dinuclear counterparts **13** and **14**: For the trinuclear systems the ν(CN) values are 40−45 cm^{-1} higher and come close to those of the free metallocyanides **4** and **5**. This demonstrates reduced π-backdonation from the terminal metals to the cyanide ligands, corresponding with the fact that in the trinuclear systems two L_nM−CN "ligands" satisfy the acceptor properties of the central (salene)Fe^{III} units. The validity of this argument is supported by two further observations: Firstly the monomeric dinuclear complex **12** shows its CN band 30 cm^{-1} higher than its water-free counterpart **14**, secondly the dimeric and tetranuclear complexes **13** and **14** show ν(CN) values that are close to those of their trinuclear analogs **19** and **20**. In all these species with clearly octahedral coordination of the central Fe^{III}, the ν(CN) values are high, while for **13** and **14** in solution they are low. A consistent interpretation thus requires that **13a**, **13b** and **14** are five-coordinate in solution, i.e. have only one donor ligand for Fe^{III} in addition to the salene ligand.

Electrochemistry

All new complexes were subjected to cyclic voltammetry in dichloromethane solution. As previously observed, it was found that the species with carbonyl ligands (**15**−**18**, **21**−**23**) do not yield reversible redox waves and lead to electrode coating. All other compounds, however, showed a reversible multistep redox behavior that allowed a consistent interpretation of their electronic nature and of their metal−metal interactions. The corresponding data are listed in Table 2.

Table 2. Cyclic-voltammetry data

	L_nM'[b]	red. Fe^{III}	ox(1) L_nM	ox(2) L_nM
4	Cp(dppe)Fe		0.48	
5	$Cp(PPh_3)_2Ru$		0.79	
[**12**]SbF_6	$Cp(PPh_3)_2Ru$	−0.30	1.08	
[**13a**]PF_6	Cp(dppe)Fe	−0.34	0.86	
[**13b**]PF_6	Cp(dppe)Fe	−0.31	0.82	
[**14**]PF_6	$Cp(PPh_3)_2Ru$	−0.32	1.12	
[**19a**]PF_6	Cp(dppe)Fe	−0.35	0.46	0.86
[**20a**]PF_6	$Cp(PPh_3)_2Ru$	−0.39	0.89	1.12[c]

[a] In dichloromethane, scan speed 100 mV/s, potentials in V vs. Ag/AgCl. − [b] Terminal organometallic unit. − [c] Irreversible.

In all oligonuclear complexes the reduction of the central Fe^{III} ion occurs within the very narrow potential range of −0.32 to −0.39 V. This points to a very good balance of electron acceptance by the central iron and electron donation by its one or two axial ligands. As an example, the water molecule and the Ru−CN ligand in **12** have about the same effect as the single Ru−CN ligand in **14**. This implies that the Ru−CN ligand in **14** must donate more

electron density than that in **12**, which is clearly evident from the IR data and, to a lesser extent, also from the redox potentials of the Ru−CN units in **12** and **14**. The inherent implication that the 1:1 complexes **13** and **14** are monomeric, i.e. dinuclear, in solution is borne out by the simplicity of their cyclic voltammograms, which for the corresponding tetranuclear complexes should show at least one more redox wave due to the stepwise reduction of the two closely spaced, i.e. strongly interacting, central Fe^{III} centers.

The increase of the redox potentials of the cyanometal "ligands" **4** and **5** upon single coordination to the (salene)-Fe^{III} unit amounts to 0.3−0.4 V. This is somewhat larger than observed previously for related dinuclear complexes,[1,2,4,5] and corresponds to the considerable withdrawal of electron density through π-backdonation as diagnosed above from the IR data. In this respect the pair of complexes **13a/13b** provides an internal test for the mutual effects of the shift of electron density between the two redox centers across the cyanide bridge. In **13a** the (salene)Fe^{III} unit is more difficult to reduce (i.e. more electron-rich) and, in addition, the Cp(dppe)Fe unit is more difficult to oxidize (i.e. more electron-poor) than their counterparts in **13b**.

In the trinuclear complexes **19a** and **20a** the Fe^{III} centers are slightly more difficult to reduce than in the dinuclear complexes, corresponding to their higher electron density due to the presence of two cyanometal donors. On the other hand, the first oxidative waves appear at significantly lower potentials than in the dinuclear complexes. This agrees again with the observations from the IR data, which indicate a significantly smaller π-backdonation from the outer organometallic units in **19a** and **20a**. Figure 4 shows the two voltammograms.

The most important feature of the trinuclear complexes **19a** and **20a** is the occurrence of two well-separated oxidative waves in their voltammograms. These must represent the stepwise oxidation of the two outer organometallic units. At first glance the two oxidation potentials in both cases are conspicuously close to those of the dinuclear complexes (**13a**, **14**) plus the two free metallocyanides (**4**, **5**), leading to the suspicion that **19a** and **20a** dissociate into these components in solution. However, these components should be detectable in the IR spectra and (for **4** and **5**) by NMR, which was not the case. Thus, the large separation of the redox waves must be taken as being real and as an indication of a strong electronic interaction between the two outer organometallic units which are ca. 10 Å apart. The extent of this interaction, as measured by the potential separation, is unusually large when compared to that in related trinuclear $(M'-CN)_2M$ complexes investigated by other researchers[15−17] and ourselves.[2][4]

It seemed feasible that the isolation of the mono-oxidized species [**19a**]X_2 or [**20a**]X_2 should be possible after chemical oxidation or controlled potential electrolysis. These species would be valuable for probing the long-range metal−metal interactions by optically induced MMCT as described in the following section. However, various attempts to generate these species chemically or electrolytically, or even to spectroscopically prove their existence in solution, met with failure.

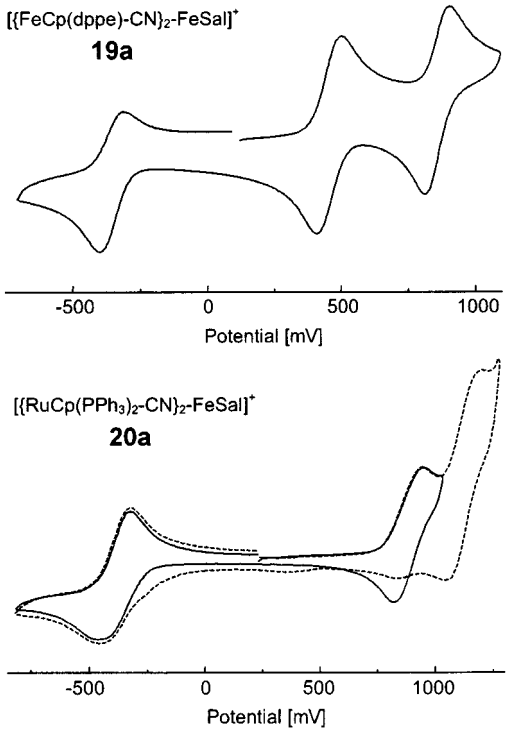

Figure 4. Cyclic voltammograms of **19a** and **20a** (for details see Table 2); for **20a** the solid line corresponds to a scan range of −0.80 to +1.05 V, the dashed line to a scan range of −0.80 to +1.35 V

Metal−Metal Charge Transfer

The phenomenon of optically induced metal−metal charge transfer (MMCT) finds its popular representation in the name Prussian Blue (generally accepted for a class of compounds of approximate composition $M^IFe^{II}Fe^{III}(CN)_6 \cdot x\ H_2O$, corresponding to an MMCT absorption at 680 nm. The practical relevance of this has led to many investigations of the optical properties of coordination compounds containing cyanide-bridged metal centers.[3] Few of those, however, reproduce the electronic situation in Prussian Blue, which contains Fe^{III} as a d^5 high-spin species attached to the N terminus and Fe^{II} as a d^6 low-spin species attached to the C terminus of the cyanide bridge. All complexes described here have just this configuration and thus are simple low-molecular representatives of Prussian Blue.

The optical properties of the complexes yield partial justification for this statement. Table 3 lists the UV/Vis absorption of the analytically pure compounds (except **15**−**17**, which are insoluble in dichloromethane). It is evident that the spectra are dominated by the LMCT absorptions in the visible range, of which those due to the (salene)Fe^{III} units are 5 to 10 times as intense as those due to the organometallic units. For the di- and trinuclear complexes containing carbonyl ligands on the organometallic units (**18**, **21**−**23**) there are no further spectral features, leading to the conclusion that a possible MMCT from the outer metal centers

to the central Fe^{III} is too high in energy to be discernable from the LMCT, in accord with the high redox potentials of these outer organometallic groups.

Table 3. UV/Vis data {in dichloromethane, $\lambda_{max}(\varepsilon_{max})$ [nm(M^{-1} cm^{-1})]}

	L_nM'[a]	LMCT	MMCT
1a	–	474(4300)	
1b	–	453(3800), 512(3600)	
3	$Cp(CO)_2Fe$	348(830)	
4	Cp(dppe)Fe	409(620)	
5	$Cp(PPh_3)_2Ru$	330(300)	
[**12**]SbF_6	$Cp(PPh_3)_2Ru$	494(5800)	
[**13a**]PF_6	Cp(dppe)Fe	416(4900), 504(4950)	741(2200)
[**13b**]PF_6	Cp(dppe)Fe	492(5700), 560(6000)	796(2500)
[**14**]PF_6	$Cp(PPh_3)_2Ru$	430(4600), 497(5000)	
[**18a**]ClO_4	$Cp(CO)_2Fe$	402(4300), 504(3400)	
[**18b**]SbF_6	$Cp(CO)_2Fe$	422(5400), 495(4300)	
[**19a**]PF_6	Cp(dppe)Fe	404(5800), 500(5950)	630(3950)
[**20a**]PF_6	$Cp(PPh_3)_2Ru$	440(4400), 494(5300)	
[**21**]PPh_4	$(CO)_5Cr$	440(2600), 511(3400)	
[**22**]PPh_4	$(CO)_5Mo$	439(2900), 503(3500)	
[**23**]PPh_4	$(CO)_5W$	440(3100), 491(3600)	

[a] Terminal organometallic unit.

At first glance this also seems to be the case for the ruthenium-containing complexes **12**, **14**, and **20a**. However, their absorption intensities for the LMCT are higher and their spectral traces extend by about 100 nm further into the visible range than those of the aforementioned complexes. This situation is represented in Figure 5. It can be interpreted by a hidden MMCT absorption at ca. 550 nm. Again, the high redox potentials of the Ru centers in these complexes can serve as an explanation for the high MMCT energies.

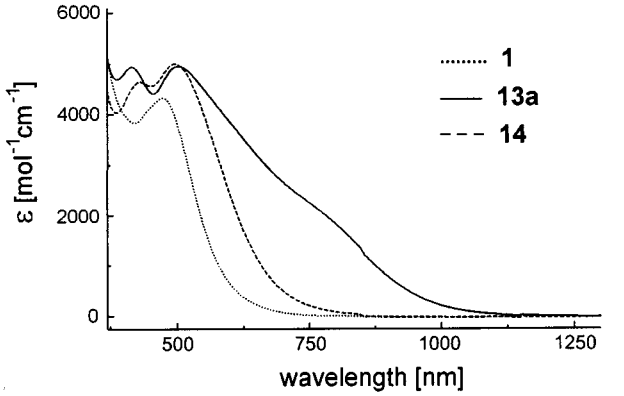

Figure 5. Superposition of the UV/Vis spectra of the reference compound **1a** and its dinuclear $Fe^{III}-NC-Fe^{II}$ and $Fe^{III}-NC-Ru^{II}$ derivatives **13a** and **14** (in CH_2Cl_2)

Only for the di- and trinuclear complexes containing Cp(dppe)Fe as the organometallic unit with the lowest redox potential on the terminal positions (**13a**, **13b**, **19a**) are the MMCT absorptions visible as shoulders in the spectra, cf. Figure 5. Compound **13b** shows the MMCT transition of lowest energy, which can be explained by the observations, mentioned above, that in **13b** both the Fe^{III} center is easier to reduce and the Fe^{II} center easier to oxidize than their counterparts in **13a**. The observation that the trinuclear complex **19a** shows an MMCT of higher energy than its dinuclear counterpart **13a**, despite the lower first redox potential of its Cp(dppe)Fe unit, cannot be explained by the simple arguments used here. It serves, however, as additional proof that **19a** does not dissociate into **13a** and **4** in solution, as suspected above. Altogether the MMCT energies of these three complexes come close enough to that of Prussian Blue to allow the statement that they represent a viable model of its high-spin-$Fe^{III}-NC-$low-spin-Fe^{II} arrangement.

The MMCT transitions observed here correspond to electronic interactions between neighboring metal centers, and in the trinuclear complexes the intramolecular redox process transfers an electron from the terminal metal centers to the central Fe^{III}. Thus, the ability of the tri- and tetranuclear species for long-range metal−metal interactions has not been exploited. This poses the challenge of either obtaining the elusive one-electron oxidation products of **19** or **20** or preparing unsymmetrical (i.e. heterotrimetallic) trinuclear complexes.

Magnetism

All new complexes contain several unpaired electrons located on the salene-bound high-spin Fe^{III} centers. Their magnetic moments were determined at room temperature by the Gouy method in order to find out how the basic magnetic properties of (salene)Fe^{III} complexes are modified by the attachment of the cyanometal "ligands" and to possibly detect new magnetic interactions. The measured values of χ_{mol} were corrected for the diamagnetic contributions,[18] and from the resulting values $c^{corr}{}_{mol}$ the magnetic moments μ_{eff} were calculated using the formula $\mu_{eff} = 2.828(\chi^{corr}{}_{mol} \cdot T)^{1/2}$. The corresponding data are listed in Table 4.

Table 4. Magnetic data at room temperature

	χ_{mol} [10^{-2} $cm^{-3}mol^{-1}$]	$\chi^{corr}mol$ [10^{-2} $cm^{-3}mol^{-1}$]	μ_{eff} [μ_B]
a) reference compounds			
1a			5.19[19]
1b			5.01[19]
b) 1:1 complexes			
[**12**]SbF_6	1.286	1.363	5.65
[**13a**]PF_6	1.168	1.229	5.37
[**13b**]SbF_6	1.119	1.189	5.27
[**14**]PF_6	1.249	1.334	5.59
15	1.141	1.169	5.23
16	1.165	1.196	5.29
17	1.151	1.185	5.27
c) 1:2 complexes			
[**18a**]ClO_4	1.291	1.327	5.58
[**18b**]SbF_6	1.181	1.231	5.37
[**19a**]PF_6	1.310	1.408	5.74
[**20a**]PF_6	1.327	1.444	5.82
[**21**]PPh_4	1.239	1.300	5.52
[**22**]PPh_4	1.263	1.330	5.58
[**23**]PPh_4	1.225	1.298	5.51

It is known that the Fe^{III} ion in salene complexes can be low-spin [e.g. (salene)$Fe(CN)_2$] or high-spin [e.g. (salene)-Fe(imidazole)$_2$][20] and that the dimeric (salene)Fe−X complexes represented by **B** show antiferromagnetic coupling between the two high-spin Fe^{III} ions, amounting, for instance, to $J = -8\ cm^{-1}$ for our reference complex **1a**.[19] Thus, there existed the possibility that the cyanometal "ligands" employed here would induce low-spin behavior or stronger magnetic coupling within the $Fe_2(salene)_2$ cores, as we have observed before for $[Fe_4S_4]^{2+}$ cores ligated by cyanometal units.[21]

As Table 4 shows, all magnetic moments are lower than the spin-only value of 5.92 μ_B for high-spin d^5. For the trinuclear 1:2 complexes this cannot be explained by antiferromagnetic coupling. It is possibly an expression of spin crossover, i. e. the presence of small amounts of low-spin species. Such an equilibrium of high-spin and low-spin Fe^{III} complexes was deduced for [(**L2**)Fe(imidazole)$_2$]BPh_4.[20] Irrespective of this it is evident that the cyanometal "ligands" are not strong enough to induce a real low-spin situation.

The lowering of the magnetic moments for the 1:1 complexes points to antiferromagnetic coupling within the $Fe_2(salene)_2$ units with the same order of magnitude as previously observed for the (salene)Fe−X dimers.[9,12,19,20] Thereby it is another indication that all complexes **13**−**17** exist as tetranuclear dimers in the solid state with structures comparable to that of **13a**. Complex **12**, which has a typically higher magnetic moment close to that of the spin-only value, underlines this, being the only monomeric 1:1 complex in the solid state due to its aqua ligand. Thus a consistent qualitative description of the magnetic properties can be achieved with the room temperature data, while a more detailed description would require low-temperature measurements.

Conclusions

The combination of (salene)Fe^{III} fragments with cyanometal units has yielded three types of arrangements: dinuclear 1:1 complexes, dimers thereof as tetranuclear 2:2 complexes, and linear trinuclear 1:2 complexes. The constitution of the tetranuclear species, which exist only in the solid state, was confirmed by a structure determination, by the IR data and the magnetic measurements. Their existence as dinuclear species in solution was deduced from the electrochemical and IR data and by reference to the structure determination of a related complex. The identity of the trinuclear species in the solid state and in solution was ascertained by the electrochemical, spectroscopic and magnetic measurements, again in combination with a crystal structure analysis.

The electronic interactions between the metal atoms across the cyanide bridges were evaluated by cyclic voltammetry and UV/Vis spectroscopy. The electrochemical measurements revealed a strong interaction between the terminal metal atoms in the linear trinuclear M−CN−Fe−NC−M arrays, the electronic spectra showed an optically induced metal−metal charge transfer from the terminal M^{II} centers to the (salene)Fe^{III} center. The electronic situation and the energy of the MMCT make the complex [(salene)Fe^{III}−NC−Fe^{II}(dppe)Cp]$^+$ (**13**) the simplest molecular analog of Prussian Blue.

In comparison to the di- and trinuclear systems previously reported by us, which were mostly organometallic complexes,[1,2,4] the compounds described here show four characteristic features: (1) They have a compositional (and structural) variability that can only partly be controlled by the synthetic approach. (2) They are labile with respect to the orientation of the CN bridge, resulting in the accessibility of only one of the two orientational isomers. (3) They show an unusually large separation of the two redox waves for the two outer, chemically equivalent, M′ units, indicating a strong electronic interaction between them. (4) They are paramagnetic and of high spin, opening the possibility to study magnetic interactions.

Experimental Section

The general working conditions, the synthesis of the organometallic reagents and the details of the measurement procedures are listed in ref.[1] Complexes **1a**, **1b**, **2a** and **2b** were prepared according to ref.[9] Magnetic susceptibilities were measured with an MSB Auto Balance, which was calibrated with $K_3[Fe(CN)_6]$. Analytical data for the new complexes are given in Table 5.

[12]PF_6: 0.500 g (1.20 mmol) of **1b** and 0.858 g (1.20 mmol) of **5** in 50 mL of methanol were heated to 50°C for 2 h and then filtered hot. After addition of 0.195 g (1.20 mmol) of NH_4PF_6, the mixture was stirred at 50°C for 30 min and again filtered hot. The filtrate was kept in an open beaker until about half of the solvent had evaporated. The precipitate was filtered off, washed with ether and dried in a stream of nitrogen to yield 487 mg (30%) of [**12**]PF_6 as black crystals, m.p. 230°C (dec.).

[12]SbF_6: This compound was obtained in the same way from 0.500 g (1.20 mmol) of **1b**, 0.858 g (1.20 mmol) of **5** and 0.310 g (1.20 mmol) of $NaSbF_6$. Yield 504 mg (31%) of [**12**]SbF_6 as black crystals, m.p. 230°C (dec.).

[13a]ClO_4: 104 mg (0.29 mmol) of **1a** and 159 mg (0.29 mmol) of **4** in 50 mL of methanol were stirred at 50°C for 2 h, filtered hot, treated with 31 mg (0.29 mmol) of $LiClO_4$, stirred at 50°C for 30 min and filtered hot. Slow cooling to room temperature (12 h) led to the precipitation of 126 mg (45%) of [**13a**]ClO_4 as black crystals, m.p. 220°C (dec.), which were washed with ether and dried in a stream of nitrogen.

[13a]PF_6: This compound was obtained in the same way from 204 mg (0.57 mmol) of **1a**, 311 mg (0.57 mmol) of **4** and 93 mg (0.57 mmol) of NH_4PF_6. Yield 192 mg (33%) of [**13a**]PF_6, black crystals, m.p. 220°C (dec.).

[13a]BPh_4: This compound was obtained in the same way from 212 mg (0.59 mmol) of **1a**, 324 mg (0.59 mmol) of **4** and 203 mg (0.59 mmol) of $NaBPh_4$. Yield 312 mg (44%) of [**13a**]BPh_4, black crystals, m.p. 180°C (dec.).

[13a]SbF_6: This compound was obtained in the same way from 195 mg (0.55 mmol) of **1a**, 298 mg (0.55 mmol) of **4** and 141 mg (0.55 mmol) of $NaSbF_6$. Yield 235 mg (39%) of [**13a**]SbF_6, black crystals, m.p. 225°C (dec.).

[13b]PF_6: This compound was prepared in the same way as [**12**]PF_6 from 152 mg (0.36 mmol) of **1b**, 199 mg (0.36 mmol) of **4** and 59 mg (0.36 mmol) of NH_4PF_6 in 70 mL of methanol. Yield 103 mg (26%) of [**13b**]PF_6 as black crystals, m.p. 200°C (dec.).

[13b]SbF_6: This compound was prepared in the same way as described above, from 107 mg (0.26 mmol) of **1b**, 140 mg (0.26 mmol) of **4** and 66 mg (0.26 mmol) of $NaSbF_6$. Yield 89 mg (30%) of [**13b**]SbF_6 as black crystals, m.p. 190°C (dec.).

[14]ClO_4: This compound was prepared in the same way as [**12**]PF_6, from 113 mg (0.32 mmol) of **1a**, 226 mg (0.32 mmol) of **5** and 34 mg (0.32 mmol) of $LiClO_4$. Yield 153 mg (42%) of [**14**]ClO_4, black crystals, m.p. 230°C (dec.).

[14]PF_6: This compound was prepared in the same way as described above, from 154 mg (0.43 mmol) of **1a**, 309 mg (0.43 mmol) of **5** and 35 mg (0.43 mmol) of NH_4PF_6. Yield 253 mg (50%) of [**14**]PF_6, black crystals, m.p. 240°C (dec.).

[14]SbF_6: This compound was prepared in the same way as described above, from 207 mg (0.58 mmol) of **1a**, 415 mg (0.58 mmol) of **5** and 150 mg (0.58 mmol) of $NaSbF_6$. Yield 279 mg (38%) of [**14**]SbF_6, black crystals, m.p. 240°C (dec.).

[14]BPh_4: This compound was prepared in the same way as described above, from 100 mg (0.28 mmol) of **1a**, 200 mg (0.28 mmol) of **5** and 96 mg (0.28 mmol) of $NaBPh_4$. Yield 178 mg (47%) of [**14**]BPh_4, black crystals, m.p. 200°C (dec.).

15: 200 mg (0.56 mmol) of **1a** and 135 mg (0.58 mmol) of **6** in 100 mL of methanol were stirred at 50°C for 2 h. After cooling to room temperature, the mixture was filtered. The precipitate was washed 3 times with 20 mL of cold methanol and then with 20 mL of ether and dried in vacuo, leaving 123 mg (41%) of **15** as a blue-purple powder, m.p. 130°C. − IR (CH_3OH): $\tilde{\nu}$(CO) = 1907 cm^{-1} m, 1934 s, 2053 m.

16: This compound was prepared in the same way as described above, from 296 mg (0.83 mmol) of **1a** and 236 mg (0.83 mmol) of **7**. Yield 164 mg (34%) of **16** as a purple powder, m.p. 140°C. − IR (CH_3OH): $\tilde{\nu}$(CO) = 1910 cm^{-1} m, 1937 s, 2058 m.

17: This compound was prepared in the same way as described above, from 303 mg (0.85 mmol) of **1a** and 316 mg (0.85 mmol) of **8**. Yield 206 mg (36%) of **17** as a red-brown powder, m.p. 145°C. − IR (CH_3OH): $\tilde{\nu}$(CO) = 1902 cm^{-1} m, 1929 s, 2058 m.

[18a]PF_6 from 1a: 149 mg (0.42 mmol) of **1a** and 169 mg (0.83 mmol) of **3** were stirred in 50 mL of methanol at 50°C for 2 h. After a hot filtration, 68 mg (0.42 mmol) of NH_4PF_6 was added and the mixture stirred at 50°C for 30 min. After filtration, the solvent was removed in vacuo, the residue taken up in 30 mL of dichloromethane, the solution filtered and then layered with 60 mL of petroleum ether (b.p. 60−70°C). 161 mg (44%) of [**18a**]PF_6 was separated as brown crystals, m.p. 180°C (dec.), which were filtered off, washed with 20 mL of petroleum ether and dried in a stream of nitrogen. − IR (CH_2Cl_2): $\tilde{\nu}$(CO) = 2024 cm^{-1} s, 2065 s.

[18a]ClO_4: This compound was prepared in the same way as described above, from 101 mg (0.28 mmol) of **1a**, 115 mg (0.57 mmol) of **3** and 30 mg (0.28 mmol) of $LiClO_4$. Yield 122 mg (52%) of [**18a**]ClO_4, brown crystals, m.p. 180°C (dec.). − IR (CH_2Cl_2): $\tilde{\nu}$(CO) = 2024 cm^{-1} s, 2065 s.

[18a]SbF_6: This compound was prepared in the same way as described above, from 150 mg (0.42 mmol) of **1a**, 170 mg (0.84 mmol) of **3** and 109 mg (0.42 mmol) of $NaSbF_6$. Yield 167 mg (41%) of [**18a**]SbF_6, brown crystals, m.p. 180°C (dec.). − IR (CH_2Cl_2): $\tilde{\nu}$(CO) = 2024 cm^{-1} s, 2065 s.

[18a]BPh_4: This compound was prepared in the same way as described above, from 175 mg (0.49 mmol) of **1a**, 199 mg (0.98 mmol) of **3** and 167 mg (0.49 mmol) of $NaBPh_4$. Yield 219 mg (43%) of [**18a**]BPh_4, brown powder, m.p. 165°C (dec.). − IR (CH_2Cl_2): $\tilde{\nu}$(CO) = 2024 cm^{-1} s, 2065 s.

[18a]PF_6 from 2a: 230 mg (0.56 mmol) of **2a** and 41 mg (1.12 mmol) of **9** in 50 mL of methanol were stirred at room temp. for 12 h. 92 mg (0.56 mmol) of NH_4PF_6 was added, the mixture stirred for another 5 h and then filtered. The filtrate was concentrated to dryness, the residue taken up in 20 mL of dichloromethane, the solution filtered and the filtrate layered with 60 mL of petroleum ether (b.p. 60−70°C). The resulting precipitate consisted of **3** and

Table 5. Analytical characterization

	Empirical formula Molecular mass	Analyses calcd./found C	 H	 N
[**12**]PF_6	$C_{60}H_{55}F_6FeN_3O_5P_3Ru$	57.11	4.39	3.33
	1261.94	56.61	4.32	3.28
[**12**]SbF_6	$C_{60}H_{55}F_6FeN_3O_5P_2RuSb$	53.28	4.10	3.11
	1352.71	53.19	4.04	3.14
[**13a**]ClO_4	$C_{48}H_{43}ClFe_2N_3O_6P_2$	59.62	4.48	4.35
	966.98	59.38	4.56	4.36
[**13a**]PF_6	$C_{48}H_{43}F_6Fe_2N_3O_2P_2$	56.94	4.28	4.15
	1012.49	56.66	4.26	4.13
[**13a**]BPh_4	$C_{72}H_{63}BFe_2N_3O_2P_2$	72.87	5.35	3.54
	1186.76	72.66	5.28	3.53
[**13b**]PF_6	$C_{50}H_{47}F_6Fe_2N_3O_4P_3$	55.99	4.42	3.92
	1072.54	55.24	4.47	3.98
[**13b**]SbF_6	$C_{50}H_{47}F_6Fe_2N_3O_4P_2Sb$	51.62	4.07	3.61
	1163.32	50.75	4.07	3.64
[**14**]ClO_4	$C_{58}H_{49}ClFeN_3O_6P_2Ru$	61.20	4.34	3.69
	1138.36	60.38	4.28	3.74
[**14**]PF_6	$C_{58}H_{49}F_6FeN_3O_2P_3Ru$	58.84	4.17	3.55
	1183.87	58.65	4.07	3.51
[**14**]SbF_6	$C_{58}H_{49}F_6FeN_3O_2P_2RuSb$	54.65	3.87	3.30
	1274.65	54.48	3.72	3.22
[**14**]BPh_4	$C_{82}H_{69}BFeN_3O_2P_2Ru$	72.52	5.12	3.09
	1358.14	72.15	5.07	3.09
15	$C_{22}F_{14}CrFeN_3O_7$	48.91	2.61	7.78
	540.21	48.78	2.61	7.62
16	$C_{22}H_{14}FeMoN_3O_7$	45.23	2.42	7.19
	584.16	45.32	2.30	6.44
17	$C_{22}H_{14}FeN_3O_7W$	39.32	2.10	6.25
	672.07	40.30	2.34	6.08
[**18a**]PF_6	$C_{32}H_{24}F_6Fe_3N_4O_6P$	44.02	2.77	6.42
	873.07	44.88	3.05	6.12
[**18a**]ClO_4	$C_{32}H_{24}ClFe_3N_4O_{10}$	46.44	2.92	6.77
	827.56	46.18	2.93	6.53
[**18a**]SbF_6	$C_{32}H_{24}F_6Fe_3N_4O_6Sb$	39.88	2.51	5.81
	963.84	41.60	2.52	5.92
[**18a**]BPh_4	$C_{56}H_{44}BFe_3N_4O_6$	64.22	4.66	5.98
	1047.34	63.20	4.13	6.03
[**18b**]SbF_6	$C_{34}H_{28}F_6Fe_3N_4O_8Sb\cdot$ 1.5 CH_2Cl_2	37.04	2.71	4.87
	1151.30	36.74	2.93	5.77
[**19a**]PF_6	$C_{80}H_{72}F_6Fe_3N_4O_2P_5\cdot$ 2 CH_3OH	60.72	4.97	3.45
	1621.96	59.67	4.73	3.50
[**20a**]PF_6	$C_{100}H_{84}F_6FeN_4O_2P_5Ru_2\cdot$ 1.5 CH_3OH	62.56	4.65	2.88
	1948.70	62.10	4.57	2.91
[**20a**]SbF_6	$C_{100}H_{84}F_6FeN_4O_2P_4Ru_2Sb\cdot$ 1.5 CH_3OH	59.78	4.45	2.75
	2039.47	59.11	4.25	2.76
[**21**]PPh_4	$C_{52}H_{34}Cr_2FeN_4O_{12}P$	56.90	3.12	5.10
	1097.67	55.78	3.30	4.82
[**22**]PPh_4	$C_{52}H_{34}FeMo_2N_4O_{12}P$	52.68	3.89	4.73
	1185.56	52.63	3.11	3.75
[**23**]PPh_4	$C_{52}H_{34}FeN_4O_{12}PW_2$	45.88	2.52	4.12
	1361.38	46.70	2.75	3.81

[**18a**]PF_6. After three crystallizations from dichloromethane/petroleum ether (1:3), 134 mg (55%) of pure [**18a**]PF_6 was obtained.

[18b]SbF_6 from 1b: This compound was prepared in the same way as described above for [**18a**]PF_6, from 155 mg (0.37 mmol) of **1b**, 151 mg (0.74 mmol) of **3** and 96 mg (0.37 mmol) of $NaSbF_6$. Yield 116 mg (27%) of [**18b**]$SbF_6 \cdot 1.5\ CH_2Cl_2$ as a dark brown powder with m.p. 180°C (dec.). − IR (CH_2Cl_2): $\tilde{\nu}$(CO) = 2014 cm^{-1} s, 2060 s.

[18b]SbF_6 from 2b: This compound was prepared in the same way as described above for [**18a**]PF_6, from 235 mg (0.50 mmol) of **2b**, 396 mg (1.01 mmol) of **9** and 130 mg (0.50 mmol) of $NaSbF_6$. Yield 125 mg (43%) of [**18b**]$SbF_6 \cdot 1.5\ CH_2Cl_2$.

[19a]PF_6: This compound was prepared in the same way as described above for [**18a**]PF_6, from 115 mg (0.28 mmol) of **2a**, 358 mg (0.56 mmol) of **10** and 46 mg (0.28 mmol) of NH_4PF_6. Yield 74 mg (33%) of [**19a**]$PF_6 \cdot 2\ CH_3OH$ as black crystals with m.p. 180°C (dec.).

[19b]SbF_6: This compound was prepared in the same way as described above for [**18a**]PF_6, from 225 mg (0.48 mmol) of **2b**, 614 mg (0.96 mmol) of **10** and 124 mg (0.48 mmol) of $NaSbF_6$. The recrystallization procedure yielded 50 mg (15%) of [**19b**]SbF_6 as a black powder that contained ca. 10% of impurities.

[20a]PF_6 from 1a: This compound was prepared in the same way as described above for [**12**]PF_6, from 100 mg (0.28 mmol) of **1a**, 401 mg (0.56 mmol) of **5** and 46 mg (0.28 mmol) of NH_4PF_6. Yield 84 mg (15%) of [**20a**]$PF_6 \cdot 1.5\ CH_3OH$ as black crystals of m.p. 190°C (dec.).

[20a]SbF_6: This compound was prepared in the same way as described above, from 150 mg (0.42 mmol) of **1a**, 601 mg (0.84 mmol) of **5** and 109 mg (0.42 mmol) of $NaSbF_6$. Yield 125 mg (15%) of [**20a**]$SbF_6 \cdot 1.5\ CH_3OH$, black crystals, m.p. 190°C (dec.).

[20a]PF_6 from 2a: 230 mg (0.56 mmol) of **2a** and 813 mg (1.12 mmol) of **11** in 50 mL of methanol were stirred at room temp. for 12 h. 92 mg (0.56 mmol) of NH_4PF_6 was added and the mixture stirred for another 5 h. After filtration, the filtrate was kept in a refrigerator, which led to the precipitation of a small amount of [**14**]PF_6. Slow concentration of the remaining solution yielded 135 mg (25%) of [**20a**]$PF_6 \cdot 1.5\ CH_3OH$, which was filtered off, washed with 20 mL of ether and dried in a stream of nitrogen.

[20b]SbF_6: This compound was prepared in the same way as described above for [**18a**]PF_6, from 225 mg (0.48 mmol) of **2b**, 696 mg (0.96 mmol) of **11** and 124 mg (0.48 mmol) of $NaSbF_6$. Yield 75 mg (14%) of crude [**20b**]SbF_6 as a black powder that contained ca. 15% of impurities.

[21]PPh_4: 200 mg (0.56 mmol) of **1a**, 271 mg (1.13 mmol) of **6** and 50 mL of methanol were stirred at 50°C for 2 h. After cooling to room temperature, the precipitate of **15** was filtered off. The filtrate was treated with 211 mg (0.56 mmol) of PPh_4Cl and stirred for 30 min at 50°C. After filtration, the solution was concentrated to dryness, the residue taken up in 20 mL of dichloromethane and layered with 50 mL of petroleum ether (b.p. 60−70°C). Within a few days, 135 mg (22%) of [**21**]PPh_4 had precipitated as dark purple needles, m.p. 135°C (dec.), which were filtered off, washed with 20 mL of petroleum ether and dried in a stream of nitrogen. − IR (CH_3OH): $\tilde{\nu}$(CO) = 1905 cm^{-1} m, 1935 s, 2058 m.

[22]PPh_4: This compound was prepared in the same way as described above for [**21**]PPh_4, from 200 mg (0.56 mmol) of **1a**, 319 mg (1.12 mmol) of **7** and 210 mg (0.56 mmol) of PPh_4Cl. Yield 175 mg (26%) of [**12**]PPh_4, red-brown needles, m.p. 150°C (dec.). − IR (CH_3OH): $\tilde{\nu}$(CO) = 1910 cm^{-1} m, 1938 s, 2059 m.

[23]PPh_4: This compound was prepared in the same way as described above for [**21**]PPh_4, from 200 mg (0.56 mmol) of **1a**, 417 mg (1.12 mmol) of **8** and 210 mg (0.56 mmol) of PPh_4Cl. Yield 163 mg (21%) of [**23**]PPh_4, brown powder, m.p. 140°C (dec.). − IR (CH_3OH): $\tilde{\nu}$(CO) = 1904 cm^{-1} m, 1930 s, 2057 m.

Structure Determinations:[22] The crystals were obtained directly from the reaction solutions. Diffraction data were recorded at room

Table 6. Crystallographic details

	[**12**]SbF_6	[**13a**]PF_6	[**13a**]BPh_4	[**20a**]PF_6·1.5 MeOH
Empirical formula	$C_{60}H_{55}F_6FeN_3O_5P_2RuSb$	$C_{96}H_{86}F_{12}Fe_4N_6P_4P_6$	$C_{144}H_{126}B_2Fe_4N_6O_4P_4$	$C_{100}H_{84}F_6FeN_4O_2P_5Ru_2$· 1.5 CH_3OH
Molecular mass	1352.7	2024.9	2373.4	1948.7
Crystal size [mm]	0.5 × 0.5 × 0.2	0.8 × 0.4 × 0.2	0.7 × 0.5 × 0.2	0.6 × 0.4 × 0.4
Space group	$P2_1/n$	$P-1$	$P-1$	$P-1$
Z	4	1	1	2
a [Å]	14.128(4)	12.487(3)	12.679(2)	14.458(3)
b [Å]	27.902(3)	13.345(3)	14.676(2)	15.178(3)
c [Å]	14.931(3)	15.029(3)	17.490(2)	22.412(4)
α [°]	90	108.27(2)	101.92(1)	80.24(3)
β [°]	100.74(2)	100.94(2)	90.14(1)	71.08(3)
γ [°]	90	94.07(2)	106.64(1)	89.55(3)
V [$Å^3$]	5783(2)	2312.0(9)	3044.4(7)	4579(1)
d(calcd.) [g cm^{-3}]	1.55	1.45	1.30	1.41
μ(Mo-$K_α$) [mm^{-1}]	1.10	0.80	0.58	0.64
hkl range	h: 0 to 17 k: 0 to 34 l: −18 to 18	h: −14 to 14 k: −15 to 15 l: 0 to 17	h: −14 to 0 k: −17 to 17 l: −20 to 21	h: −18 to 0 k: −18 to 18 l: −27 to 26
Refl. measd.	11903	8342	11349	19349
Indep. refl.	11357	8009	10835	18583
Obs. refl. [$I > 2\ σ(I)$]	6914	2996	5363	12496
Parameters	712	578	739	1117
Refl. refined	11357	8009	10835	18583
R_1 (obs.refl.)	0.079	0.118	0.065	0.048
wR_2 (all refl.)	0.280	0.454	0.167	0.137
Residual el. density [$e/Å^3$]	+1.5 −1.3	+1.1 −0.9	+0.8 −0.4	+1.1 −1.1

temperature using the ω/2θ technique with a Nonius CAD4 diffractometer fitted with a molybdenum tube (K, $\lambda = 0.7107$ Å) and a graphite monochromator. Empirical absorption corrections based on ψ scans were applied. The structures were solved with direct methods and refined anisotropically with the SHELX program suite.[23] Hydrogen atoms were included with fixed distances and isotropic temperature factors 1.2 times those of their attached atoms. Parameters were refined against F^2. The R values are defined as $R_1 = \Sigma|F_o - F_c|/\Sigma F_o$ and $wR_2 = \{\Sigma[w(F_o^2 - F_c^2)^2]\Sigma[w(F_o^2)^2]\}^{1/2}$. Drawings were produced with SCHAKAL.[24] Table 6 lists the crystallographic data.

Acknowledgments

This work was supported by the Deutsche Forschungsgemeinschaft (Graduiertenkolleg "Ungepaarte Elektronen") and by the Fonds der Chemischen Industrie.

[1] N. Zhu, H. Vahrenkamp, *Chem. Ber.* **1997**, *130*, 1241−1252.
[2] G. N. Richardson, U. Brand, H. Vahrenkamp, *Inorg. Chem.* **1999**, *38*, 3070−3079.
[3] H. Vahrenkamp, A. Geiß, G. N. Richardson, *J. Chem. Soc., Dalton Trans.* **1997**, 3643−3651.
[4] N. Zhu, H. Vahrenkamp, *J. Organomet. Chem.* **1999**, *573*, 67−72.
[5] G. N. Richardson, H. Vahrenkamp, *J. Organomet. Chem.*, in print.
[6] A. Geiß, M. Keller, H. Vahrenkamp, *J. Organomet. Chem.* **1997**, *541*, 441−443.
[7] M. Hanack, J. Metz, *J. Am. Chem. Soc.* **1983**, *105*, 828−830.
[8] M. D. Hobday, T. C. Smith, *Coord. Chem. Rev.* **1972**, *9*, 311−337.
[9] M. Gulotti, L. Casella, A. Pasini, R. Ugo, *J. Chem. Soc., Dalton Trans.* **1977**, 339−345.
[10] M. Gerloch, F. E. Mabbs, *J. Chem. Soc.* **A 1967**, 1900−1908.
[11] M. Calligaris, G. Nardin, L. Randaccio, *Coord. Chem. Rev.* **1972**, *7*, 385−403.
[12] Y. Nishida, S. Oshio, S. Kida, *Chem. Lett.* **1975**, 79−80.
[13] H. J. Buser, D. Schwarzenbach, W. Peter, A. Ludi, *Inorg. Chem.* **1977**, *16*, 2704−2710.
[14] M. J. Scott, R. H. Holm, *J. Am. Chem. Soc.* **1994**, *116*, 11357−11367.
[15] F. L. Atkinson, A. Christophides, N. G. Connelly, H. J. Lawson, A. C. Loyns, A. G. Orpen, G. M. Rosair, G. H. Worth, *J. Chem. Soc., Dalton Trans.* **1993**, 1441−1450; N. C. Brown, G. B. Carpenter, N. G. Connelly, J. G. Crossley, A. Martin, A. G. Orpen, L. Rieger, P. H. Rieger, G. Worth, *J. Chem. Soc., Dalton Trans.* **1996**, 3977−3984.
[16] M. Zhou, W. Pfennig, J. Steiger, D. van Egen, A. B. Bocarsly, *Inorg. Chem.* **1990**, *29*, 2456−2466. Y. Wu, C. Cohran, A. B. Bocarsly, *Inorg. Chim. Acta* **1994**, *226*, 251−258.
[17] B. J. Coe, T. J. Meyer, P. S. White, *Inorg. Chem.* **1995**, *34*, 3600−3609.
[18] C. J. O′Connor, *Prog. Inorg. Chem.* **1982**, *29*, 203−283.
[19] W. M. Reiff, G. J. Long, W. A. Baker, *J. Am. Chem. Soc.* **1968**, *90*, 6347−6351.
[20] Y. Nishida, S. Oshio, S. Kida, *Bull. Chem. Soc. Jpn.* **1977**, *50*, 119−122.
[21] N. Zhu, J. Pebler, H. Vahrenkamp, *Angew. Chem.* **1996**, *108*, 984−985; *Angew. Chem. Int. Ed. Engl.* **1996**, *35*, 894−895.
[22] The crystallographic data of the structures described in this paper were deposited with the Cambridge Crystallographic Data Centre as supplementary publication no. CCDC-115536 ([**12**]SbF_6), -115537 ([**13a**]PF_6), -115538 ([**13a**]BPh_4) and 115539 ([**20a**]PF_6)] Copies of these data are available free of charge from CCDC, 12 Union Road, Cambridge CB2 1EZ (Fax: int. + 44-1223/336-033; E-mail: deposit@ccdc.cam.ac.uk).
[23] G. M. Sheldrick, *SHELX-86* and *SHELXL-93*, Programs for Crystal Structure Determination, Universität Göttingen, **1986** and **1993**.
[24] E. Keller, *SCHAKAL for Windows*, Universität Freiburg, **1998**.
Received March 9, 1999
[I99096]